Chemistry and Materials

The Center for Science Innovation

Research Article

Chem. Mater. Vol. (No.) year, page

Synthesis and Electrochemical Performance of NiFe Alloy Electrocatalysts with Trisodium Citrate and Saccharin Additives for Ethanol Electrooxidation

Minda Hurulaini[1]*, Adilia Nabilah[2], Gahthan Cholid Baasyin[2], Rinda Mulmeyda[2]

[1]Department of Safety, Health and Environmental Engineering, College of Engineering, National Kaohsiung University Science and Technology, No.1, Daxue Rd, Kaohsiung City 824005, Taiwan

[2]Department of Chemistry, Faculty of Mathematics and Natural Science, Universitas Negeri Jakarta, Jl. Rawamangun Muka, Jakarta 13220, Indonesia

*Corresponding author: mindahrl1211@gmail.com

Received
18 January 2026

Received in revised form
07 May 2026

Accepted
12 May 2026

Published online
22 May 2026

DOI
https://doi.org/10.56425/cma.v5i2.133

Abstract

This study investigates the synthesis and electrochemical performance of NiFe alloy electrocatalysts prepared via thin-film electrodeposition using different additives, namely trisodium citrate and saccharin. The aim is to compare the catalytic behavior of NiFe alloys influenced by the two additives. Structural characterization through X-ray diffraction revealed a face-centered cubic (FCC) crystalline phase in both samples, while X-ray fluorescence analysis showed a Ni:Fe ratio of 1:1 in the NiFe/Cu-TSC sample and 3:1 in NiFe/Cu-Sac sample. Electrochemical impedance spectroscopy (EIS) and Tafel analysis demonstrated that the NiFe/Cu-Sac catalyst exhibited superior charge transfer properties, with a lower charge transfer resistance (R_{ct}) and a smaller Tafel slope, indicating more efficient catalytic activity. These findings suggest that saccharin serves as a more favorable additive in enhancing the electrocatalytic performance of NiFe alloys for ethanol oxidation applications.

Keywords: NiFe, additives, electrodeposition, EOR

1. Introduction

Energy is an essential need in modern life, where almost all human activities depend on it. For years, fossil fuels have been the primary energy source. However, heavy reliance on fossil fuels has led to scarcity and environmental damage due to increasing greenhouse gas emissions [1]. Therefore, the development of clean and sustainable alternative energy sources is becoming increasingly urgent. One of the technologies currently being developed is the fuel cell (FC), which is an electrochemical-based energy conversion device capable of converting chemical energy from fuel directly into electrical energy with high efficiency and low emissions [2,3]. Among the various types of FC, Direct Ethanol Fuel Cells (DEFCs) are one of the promising candidates because they use ethanol as an environmentally friendly fuel, are easily obtained from biomass, have low toxicity, and have a high energy density of 8.00 kWh/kg compared to methanol (6.10 kWh/kg) [4,5]. However, DEFCs performance is still limited due to the slow kinetics of the ethanol oxidation (EOR) reaction at the anode, mainly due to the difficulty of breaking the C–C bonds in the ethanol molecule [6]. This reaction ideally releases 12 electrons per ethanol molecule, but in practice often does not achieve conversion [7]. Therefore, an electrocatalyst is needed that is not only active and selective, but also stable and affordable.

Noble metal-based electrocatalysts such as Pt and Ru exhibit high performance but are expensive, scarce, and prone to poisoning by reaction intermediates [8]. Transition metals such as nickel (Ni) offer a more economical alternative due to their abundance and catalytic activity in alkaline media. However, Ni-only

catalysts often require high overpotentials and may suffer from surface passivation, limiting their activity.

Alloying Ni with a second transition metal is an effective strategy to enhance its catalytic performance. Among various candidates, iron (Fe) is particularly attractive due to its low cost, abundance, and strong catalytic activity in alkaline environments. Fe readily forms active oxyhydroxide species such as FeOOH, and its incorporation into Ni-based systems has been shown to modify the electronic structure, promote high-valence active sites, and enhance charge transfer kinetics. In NiFe systems, Fe also facilitates the adsorption of reaction intermediates such as *OH and *OOH, thereby improving overall catalytic efficiency [9]. These synergistic effects make NiFe alloys highly effective for alkaline electrocatalysis and promising candidates for ethanol electrooxidation (EOR).

In this work, thin-film electrodeposition was selected as a simple, low-temperature, and scalable route to directly grow NiFe on a conductive Cu substrate (NiFe/Cu). Compared with powder-based wet-chemical syntheses (e.g., hydro/solvothermal methods or co-precipitation followed by catalyst ink preparation), electrodeposition offers (i) a short synthesis time and low cost, (ii) strong adhesion and binder-free electrodes, (iii) straightforward control of deposition potential/time to tune film thickness and composition, and (iv) the ability to introduce organic additives that steer nucleation and growth, enabling systematic tailoring of morphology and the Ni/Fe ratio.

Electrodeposition enables further tuning of NiFe film growth through the use of organic additives. Saccharin, for example, acts as a crystal-growth regulator that can refine the microstructure and accelerate nucleation, leading to a more uniform deposit and smaller feature sizes [10]. Other studies have shown that saccharin can decrease the charge-transfer resistance (R_{ct}), reduce the Tafel slope, and increase the j_f/j_b ratio, which are associated with improved electrocatalytic activity and stability in ethanol oxidation [11]. In addition to saccharin, trisodium citrate ($Na_3C_6H_5O_7$, TSC) is widely used as a complexing agent and morphology controller. By forming complexes with metal ions (e.g., Ni^{2+} and Fe^{3+}/Fe^{2+}), citrate ions can regulate the effective deposition rate of each metal and promote finer, more evenly distributed deposits, which can increase the active surface area and facilitate electron transfer [12–14]. Overall, by adsorbing on the growing surface (saccharin) or complexing metal ions in solution (trisodium citrate), these additives can shift nucleation/growth pathways and relative Ni/Fe deposition rates, thereby changing morphology, composition, and structure. Such changes are expected to influence the density of accessible active sites and charge-transfer kinetics, which ultimately determines the observed EOR activity and durability.

Thus, this paper compares saccharin and trisodium citrate as additives in the electrodeposition of NiFe electrodes. We specifically evaluate how each additive modifies (i) nucleation and film growth, which governs the resulting morphology and microstructure, and (ii) the relative deposition of Ni and Fe, which determines the alloy composition and phase formation. We then correlate these additive-induced changes with key electrochemical metrics for ethanol oxidation—onset/overpotential, current density, Tafel slope, charge-transfer resistance (R_{ct}), and operational stability—to clarify how morphology and the Ni/Fe ratio contribute to enhanced EOR performance in alkaline media and to identify the more effective additive for DEFC anode catalysts.

2. Materials and Method

2.1. Materials

The chemicals used for sample preparation and electrochemical measurements were Ni(II) sulfate hexahydrate ($NiSO_4{\cdot}6H_2O$) 0.08 M, iron(II) sulfate heptahydrate ($FeSO_4{\cdot}7H_2O$) 0.02 M, boric acid (H_3BO_3) 0.4 M, saccharin 0.2 M, Trisodium citrate (TSC) anhydrous ($Na_3C_6H_5O_7$) 0.2 M, ethanol 96%, KCl 0.5 M, KOH 1 M, NaCl, distilled water, copper plate as substrate.

2.2. Synthesis of NiFe alloy electrocatalysts

NiFe alloy electrocatalysts were prepared by potentiostatic electrodeposition in a three-electrode cell. A copper plate served as the working electrode, Pt as the counter electrode, and Ag/AgCl as the reference electrode. The base electrolyte contained 0.08 M $NiSO_4{\cdot}6H_2O$, 0.02 M $FeSO_4{\cdot}7H_2O$, and 0.4 M H_3BO_3. Two plating baths were prepared by adding either 0.2 M saccharin (NiFe/Cu-Sac) or 0.2 M trisodium citrate (TSC; NiFe/Cu-TSC). Electrodeposition was conducted at a constant potential of −1.4 V vs Ag/AgCl for 20 min using an electrochemical workstation. After deposition, the electrodes were rinsed with deionized water and dried prior to characterization and electrochemical testing.

2.3. Characterizations

X-ray diffraction (XRD) was used to identify the crystalline phases of the deposited films using an X-ray diffractometer; Cu Kα radiation, λ = 1.5406 Å). X-ray fluorescence (XRF) was used to quantify the elemental composition (Ni and Fe contents) using an XRF spectrometer. Surface morphology was examined by scanning electron microscopy

2.4. Electrochemical measurements

Electrochemical measurements were performed using in a three-electrode configuration with the NiFe/Cu electrode as the working electrode, Pt as the counter electrode, and Ag/AgCl as the reference electrode. Electrochemical impedance spectroscopy (EIS) was used to evaluate charge-transfer resistance (R_{ct}) over a frequency range of 0.1 Hz–100 kHz in 0.5 M KCl. Ethanol electro-oxidation was evaluated in 1 M KOH and 0.1 M ethanol by cyclic voltammetry (CV), linear sweep voltammetry (LSV), and chronoamperometry (CA). CV was recorded from −0.75 to 0.75 V vs Ag/AgCl at a scan rate of 50 mV s^{-1}, while LSV curves were generated at 10 mV s^{-1}. CA stability tests were carried out at 0.3 V vs Ag/AgCl for 7200 s.

3. Results and Discussion

3.1. Morphology, composition, and structure analysis

X-ray fluorescence (XRF) analysis was performed to determine the elemental composition of the electrodeposited nickel and iron metals. The Ni and Fe contents of each sample are presented in Table 1**.** The NiFe/Cu-Sac sample showed a composition of approximately 76% nickel and 24% iron, indicating that the addition of saccharin led to a Ni:Fe deposition ratio of roughly 3:1, corresponding to a Ni_3Fe alloy. In contrast, the NiFe/Cu-TSC exhibited a different metal deposition ratio, with nearly equal amounts of nickel and iron. The XRF analysis recorded approximately 51% nickel and 49% iron, indicating a Ni:Fe ratio close to 1:1.

The divergence between the precursor composition and the resulting NiFe alloy is attributed to the anomalous codeposition mechanism occur in NiFe electrodeposition. This phenomenon is characterized by the preferential deposition of the less noble metal (Fe) over the more noble metal (Ni). Consequently, Fe reduction is enhanced while Ni reduction is inhibited, leading to a Ni content in the deposit that is lower than that of the initial precursor [15].

The incorporation of saccharin as an additive, possess negatively charged functional groups (S, O, and N atoms) that strengthens the interaction between metal ions and the cathode. This promotes accelerated nucleation of both Ni and Fe, resulting in a higher Ni composition compared to the use of trisodium citrate additives [16].

Table 1. XRF metal content analysis.

Sample	Ni content *(%)*	Fe content *(%)*
NiFe/Cu-Sac	75,82	24,18
NiFe/Cu-TSC	48,73	51,27

Morphological characterization of the electrodeposited NiFe alloys is presented in Fig. 1. Both samples exhibit relatively homogeneous surface coverage, although only subtle differences in microstructure can be observed at the current magnification. NiFe/Cu-TSC (Fig. 1a) displays a grain-like morphology, whereas NiFe/Cu-Sac (Fig. 1b) appears relatively smoother and more compact. However, the overall morphological contrast between the two samples is not highly pronounced. The observed variations can be associated with the role of additives during the electrodeposition process. Saccharin is known to adsorb on the growing metal surface, promoting nucleation and suppressing excessive crystal growth, which generally leads to finer and more compact deposits [10].

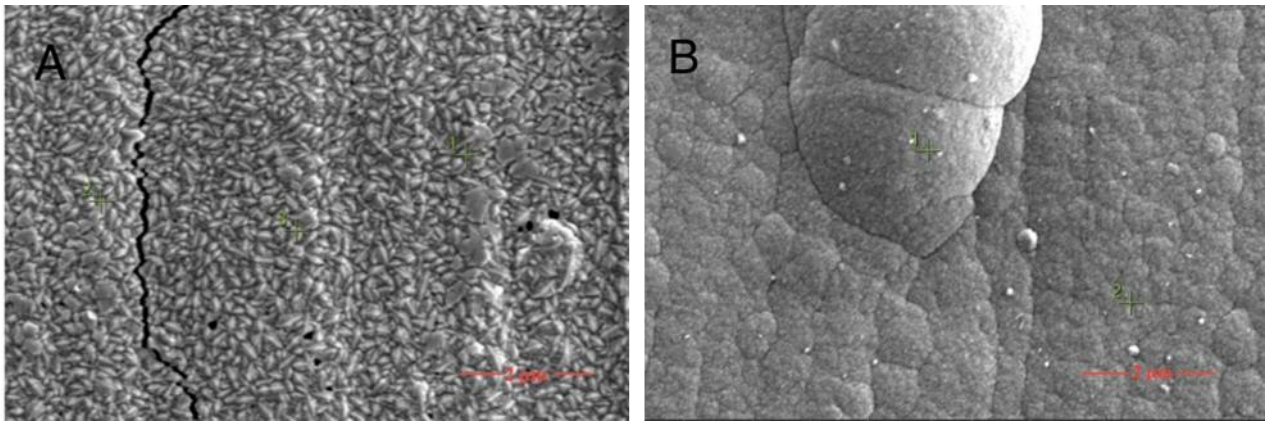

Figure 1. SEM images of NiFe (a) NiFe/Cu-TSC; (b) NiFe/Cu-Sac.

This behavior is consistent with previous reports, where the addition of saccharin resulted in smoother surfaces and reduced grain size due to enhanced nucleation and suppressed hydrogen evolution during deposition [17]. In contrast, citrate ion acts as a complexing agent in the electrolyte, influencing the relative deposition rates of Ni and Fe and potentially resulting in different grain-growth behavior [18]. These effects may contribute to the subtle differences in surface morphology observed between the samples.

It is important to note that the influence of these additives may not be fully reflected in large-scale surface features observable by SEM, but may instead manifest at the microstructural or compositional level. As shown in Table 1, NiFe/Cu-Sac exhibits a Ni-rich composition corresponding to a Ni_3Fe phase, while NiFe/Cu-TSC shows a composition closer to a 1:1 Ni:Fe ratio. Therefore, the differences in electrochemical performance are likely governed by the combined effects of alloy composition and subtle morphological variations rather than by pronounced differences in surface morphology alone.

X-ray diffraction (XRD) analysis was conducted to investigate the crystal phase structure of the NiFe alloy with the addition of TSC and saccharin additives. As shown in the diffractogram (Fig. 2), NiFe/Cu-Sac exhibited diffraction peaks at 2θ values of 51.80° and 60.58°, corresponding to the (111) and (020) Miller indices, respectively. The XRD pattern of NiFe/Cu-Sac matched with the reference pattern for Ni_3Fe from the Crystallography Open Database (COD 96-152-4834), indicating the formation of a Ni_3Fe phase. This finding was further supported by XRF analysis, which confirmed a Ni:Fe atomic ratio of approximately 3:1.

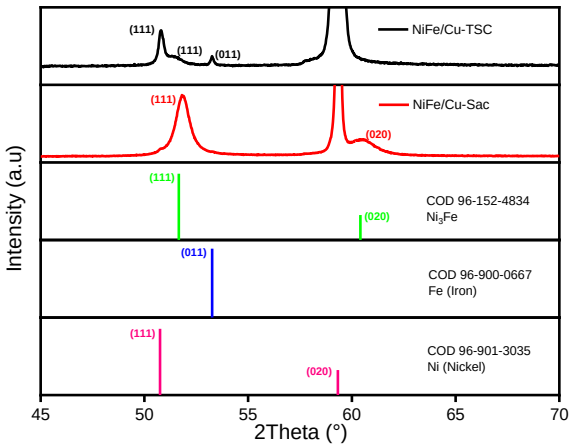

Figure 2. X-ray diffraction (XRD) patterns of NiFe/Cu-TSC and NiFe/Cu-Sac catalysts in the 2ϑ.

In contrast, the NiFe/Cu-TSC sample displayed distinct peaks at 50.78° and 53.27°, along with a broader peak at 51.51°, which correspond to the (111), (111), and (011) planes, respectively. These peaks aligned with the reference diffraction patterns of individual nickel (COD 96-901-3035) and iron (COD 96-900-0667), suggesting the presence of separated Ni and Fe phases in the alloy. These NiFe and Ni_3Fe reported to be having a cubic crystal plane on their structure [19,20].

3.2 Electrochemical analysis

Linear Sweep Voltammetry (LSV), as shown in Fig. 3a., was conducted to evaluate the electrocatalytic performance of the synthesized NiFe alloy toward ethanol electro-oxidation in an alkaline medium (KOH). The LSV measurement was performed by scanning over a defined voltage range at a constant scan rate, providing insights into the electrocatalytic behavior of the reaction, such as peak position, charge transfer current density, and enabling the determination of key parameters for electrocatalysts, including overpotential, onset potential, and Tafel slope [21,22].

The Tafel slope is widely used as a parameter to evaluate EOR kinetics, where a lower slope value indicates the catalyst's ability to accelerate the reaction with a smaller overpotential, making it an important indicator of electrocatalytic activity and efficiency [23]. The Tafel slope values were derived from the LSV curves at a scan rate of 10 mV s^{-1}. As shown in Fig. 3b, NiFe/Cu-Sac exhibits a significantly lower Tafel slope of 31 mV/dec compared to 92 mV/dec for NiFe/Cu-TSC, indicating more favorable reaction kinetics.

This enhanced performance is closely related to the morphology and composition of the NiFe/Cu-Sac sample. As observed in Fig. 1, NiFe/Cu-Sac presents a smoother and more compact surface, whereas NiFe/Cu-TSC exhibits a grain-like morphology. The finer and more uniform structure in NiFe/Cu-Sac is attributed to the role of saccharin as a growth-modifying additive, which increases nucleation and suppresses excessive crystal growth, resulting in a higher density of accessible active sites and improved ion diffusion pathways [10]. In contrast, the grain-like morphology of NiFe/Cu-TSC, influenced by citrate ion complexation, may lead to a less uniform distribution of active sites and hinder charge transport [15].

Furthermore, the Ni-rich composition of NiFe/Cu-Sac is expected to provide a higher density of Ni redox sites ($Ni(OH)_2$/NiOOH) that are active in alkaline EOR, while Fe can electronically modulate the Ni sites and enhance their catalytic properties. Therefore, the combined effects of favorable morphology and composition contribute to superior EOR kinetics, as reflected by the lower Tafel slope and charge transfer resistance observed for NiFe/Cu-Sac. In contrast, the higher Tafel slope observed for NiFe/Cu-TSC suggests a greater kinetic barrier, which can be attributed to its less favorable morphology and composition, resulting in slower electron transfer and reduced catalytic efficiency [13].

Cyclic Voltammetry (CV) testing was used to analyze the electrochemical properties of materials by observing the shape and position of the current peaks in the voltammogram. This technique provides important information regarding the electron transfer kinetics, reaction mechanisms, and redox stability of catalysts in

electrochemical systems [24]. Based on Fig. 4, in the present work, both samples exhibited a significant increase in oxidation current densities at approximately 1.5 V vs. RHE. This peak position corresponds to previous reports on the saccharin sample maintained a consistent trend of increasing current, confirming its higher surface stability compared to TSC, which began to show current stagnation after around the 80th cycle.

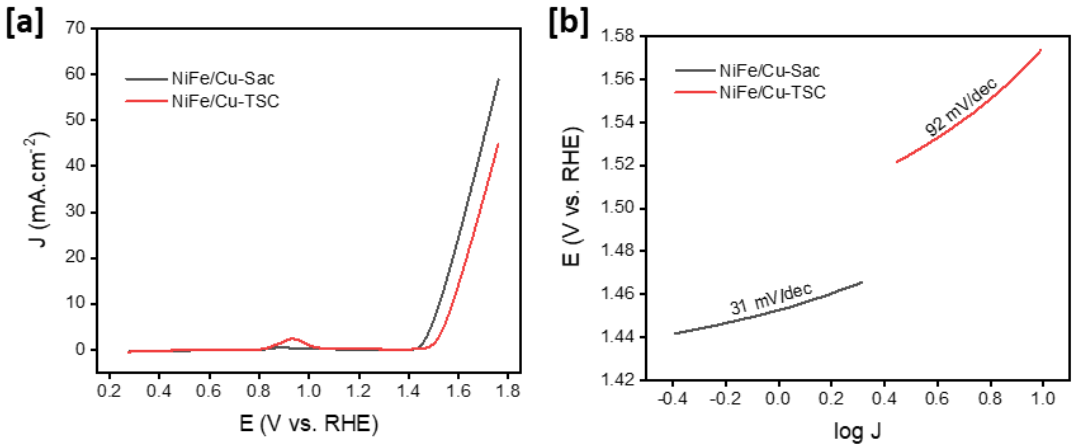

Figure 3. (a) Linear Sweep Voltammogram for NiFe/Cu-Sac and NiFe/Cu-TSC; b) Tafel plots for NiFe/Cu-Sac and NiFe/Cu-TSC.

the ethanol oxidation activity of NiFe-LDH and NiFe nanocrystalline electrocatalysts [25],[26]. This indicating that NiFe/Cu-Sac and NiFe/Cu-TSC have electrocatalytic activity towards the ethanol oxidation reaction (EOR).

However, the sample with the addition of saccharin additives showed a higher current density than TSC, indicating greater ethanol oxidation activity. This is likely due to a more active surface morphology and a more even distribution of active sites as a result of the influence of saccharin during the electrodeposition process [10]. Furthermore, the test results up to 100 cycles showed that

Electrochemical impedance spectroscopy (EIS) was conducted to evaluate the charge transfer kinetics of the synthesized NiFe samples with saccharin and trisodium citrate as additives. As illustrated in the Nyquist plot (Fig. 5), the NiFe/Cu-Sac sample exhibits a smaller semicircle diameter in the mid-frequency region, while NiFe/Cu-TSC displays a larger semicircle diameter. The diameter of the semicircle is closely related to the charge transfer resistance (R_{ct}) of the electrocatalyst sample [25]. The charge transfer resistance itself refers to the resistance encountered by ions moving from a solvated ionic state in

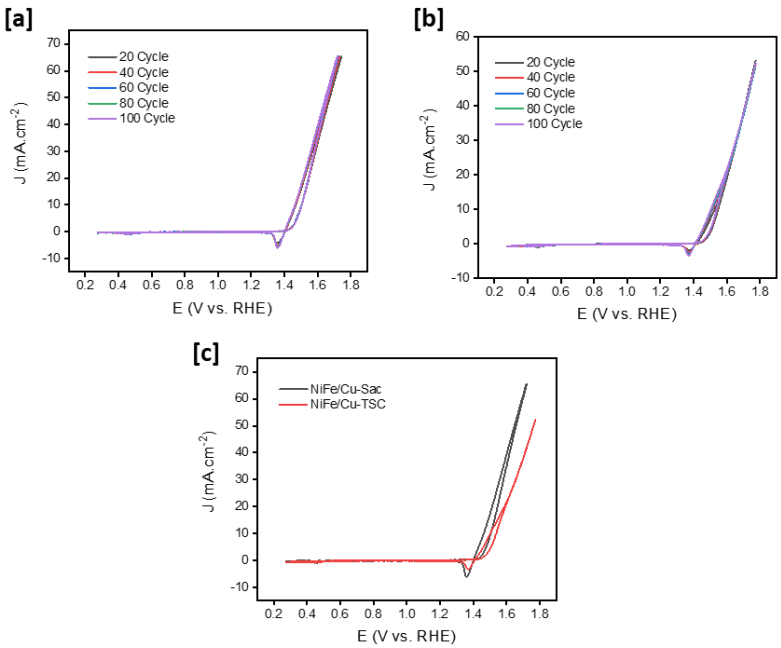

Figure 4. Cyclic voltammogram of (a) NiFe/Cu-Sac, (b) NiFe/Cu-TSC and (c) cyclic voltammogram of NiFe/Cu-Sac and NiFe/Cu-TSC at 100th cycle.

the electrolyte, across the electrode–electrolyte interface, and into the electrode material [27].

Table. 2 Charge transfer resistance (R_{ct}) of the samples.

Sample	R_{ct} (Ω)
NiFe/Cu-Sac	52.40
NiFe/Cu-TSC	203.84

As presented in Table 2, the R_{ct} values were obtained from the best-fitting Nyquist plots. NiFe/Cu-Sac demonstrates a faster charge transfer rate, as indicated by its lower R_{ct} value compared to NiFe/Cu-TSC. This lower R_{ct} value is attributed to the higher surface area of the NiFe/Cu-Sac electrode, which is a result of the addition of saccharin to the electrodeposition bath [28]. These results suggest improved electrochemical performance upon the addition of saccharin, enabling more efficient electron transfer during the ethanol electro-oxidation reaction [29].

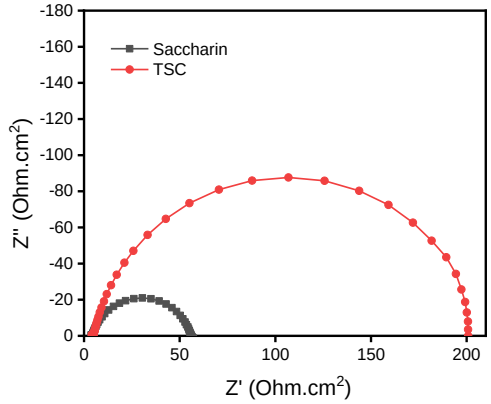

Figure 5. Nyquist plots of NiFe samples.

The activity and stability of NiFe electrocatalyst with the addition of saccharin and trisodium citrate (TSC) were tested through chronoamperometry (CA) testing at a constant potential for 7200 seconds. The CA curves shown in Fig. 6 show the current density profiles as a function of time for each sample.

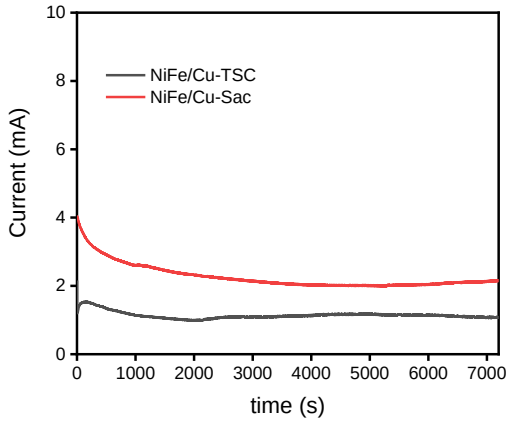

Figure 6. CA curve (current vs. time relationship) over 7200 s for NiFe/Cu-Sac and NiFe/Cu-TSC.

Figure 6 shows the NiFe catalyst synthesized with saccharin additive showed a higher initial current density (~4 mA) compared to the catalyst containing TSC (~2 mA). The current decrease in the system with saccharin was gradual and stable, reflecting good electrocatalytic performance throughout the test duration. In contrast, the NiFe/Cu-TSC experienced a sharper current decrease in the initial stage, before reaching a pseudosteady state [30]. From these results, the NiFe/Cu-Sac has a slower rate of decline and higher stability than the NiFe catalyst with addition of trisodium citrate.

The electrocatalytic performance and slower current degradation rate of NiFe/Cu-Sac indicate that saccharin acts as a crystal growth regulator agent and surface modifying additive, which is able to maintain catalytic activity and stabilize active sites against deactivation processes [31]. The slow rate of current decrease in the CA curve also reflects the catalyst's ability to maintain its structural integrity and surface activity during the electrochemical reaction process, an important characteristic of an operationally stable catalyst system. In addition, the presence of saccharin is thought to contribute to inhibiting the drastic decrease in current density by acting as a chemical barrier or surface stabilizing agent, thereby protecting the catalyst structure from contaminants or degradation due to interactions with reactive species [32].

4. Conclusion

Based on the results of characterization and electrochemical testing, it can be concluded that the addition of saccharin in the NiFe alloy electrodeposition process produces superior electrocatalytic performance compared to the use of trisodium citrate (TSC). This is evidenced by lower charge transfer resistance (R_{ct}) values, smaller Tafel slope values, higher current density in voltammetry testing, and better current stability in chronoamperometry testing. The NiFe crystal structure formed on the NiFe/Cu-Sac sample indicates saccharin's role in improving morphology and increasing the number of active surface sites. Morphological characterization through SEM reveals a noticeable difference between the two samples, with NiFe/Cu-TSC showing a more uniform grain-like morphology, while NiFe/Cu-Sac exhibits a smoother and more homogeneous surface. This morphological difference contributes to the enhancement of electrocatalytic activity, with saccharin proving to be a more effective additive in improving the performance and stability of NiFe as an electrocatalyst for ethanol oxidation reactions in Direct Ethanol Fuel Cell (DEFCs) applications. Therefore, saccharin plays a crucial role in enhancing the

performance of NiFe alloys, both in terms of activity and stability, in DEFC applications.

Author contributions

Minda Hurulaini: Investigation, Formal analysis, Methodology, Data Curation, Writing - Original Draft. **Adilia Nabilah**: Investigation, Formal analysis, Methodology, Data Curation, Writing - Original Draft. **Gahthan Cholid Baasyin**: Investigation, Formal analysis, Methodology, Data Curation, Visualization, Writing – Original. **Rinda Mulmeyda:** Writing - Review & Editing, Supervision.

Conflicts of interest

There are no conflicts to declare.

Acknowledgement

The authors would like to thank the Department of Chemistry, Faculty of Mathematics and Natural Sciences, Jakarta State University for providing laboratory facilities for this research. We also appreciate the guidance and direction from our supervisors and colleagues who have helped us during the research process and the writing of this article.

References

[1] R. Li, D. Zhou, J. Luo, W. Xu, J. Li, S. Li, P. Cheng, D. Yuan, The urchin like sphere arrays CosO4 as a bifunctional catalyst for hydrogen evolution reaction and oxygen evolution reaction, *Journal of Power Sources* **341** (2017) 250-256. https://doi.org/10.1016/j.jpowsour.2016.10.096

[2] S.W. Perng, H.W. Wu, Effects of internal flow modification on the cell performance enhancement of a PEM fuel cell, *Journal of power sources* **175** (2008) 806-816. https://doi.org/10.1016/j.jpowsour.2007.09.095

[3] E. Sokmez, I. Taymaz, E. E. Kahveci, Performance evaluation of direct ethanol fuel cell using a three-dimensional CFD model, *Fuel* **313** (2022) 123022. https://doi.org/10.1016/j.fuel.2021.123022

[4] H.R. Corti, E.R. Gonzalez, Introduction to direct alcohol fuel cells, Direct Alcohol Fuel Cells: Materials, Performance, Durability and Applications (pp. 1-32), Springer Netherlands, 2014. https://doi.org/10.1007/978-94-007-7708-8_1

[5] M.A.F. Akhairi, S. K. Kamarudin, Catalysts in direct ethanol fuel cell (DEFC): An overview, *International Journal of Hydrogen Energy* **41** (2016) 4214-4228. https://doi.org/10.1016/j.ijhydene.2015.12.145

[6] Y. Wang, S. Zou, W.B. Cai, Recent advances on electro-oxidation of ethanol on Pt-and Pd-based catalysts: from reaction mechanisms to catalytic materials, *Catalysts* **5** (2015) 1507-1534. https://doi.org/10.3390/catal5031507

[7] B. Braunschweig, D. Hibbitts, M. Neurock, A. Wieckowski, Electrocatalysis: A direct alcohol fuel cell and surface science perspective, *Catalysis Today* **202** (2013) 197- 209. https://doi.org/10.1016/j.cattod.2012.08.013

[8] C. Meng, T. Ling, Ma, H. Wang, , Z. HuZhou, Y. Mao, J.X.W. Du, M. Jaroniec, S.Z. Qiao, Atomically and electronically coupled Pt and CoO hybrid nanocatalysts for enhanced electrocatalytic performance, *Advanced Materials* **29** (2017) 1604607. https://doi.org/10.1002/adma.201604607

[9] M.P. Kumar, M. Sasikumar, A. Arulraj, V. Rajasudha, G. Murugadoss, M. R. Kumar, S G. Peera, R.V. Mangalraja, NiFe layered double hydroxide electrocatalyst prepared via an electrochemical deposition method for the oxygen evolution reaction, *Catalysts* **12** (2022) 1417. https://doi.org/10.3390/catal12111470

[10] S. Budi, B. Kurniawan, D.M. Mott, S. Maenosono, A.A. Umar, A. Manaf, Comparative trial of saccharin-added electrolyte for improving the structure of an electrodeposited magnetic FeCoNi thin film, *Thin Solid Films* **642** (2017) 51-57. https://doi.org/10.1016/j.tsf.2017.09.017

[11] R. Mulmeyda, A. G. Sidik, C.S Maura, & A. A. Fazri, The effect of saccharin on SnNi alloy: the electrodeposition and its electrocatalytic activity in ethanol oxidation reaction, *Chemistry and Materials* **33** (2024) 107-115. https://doi.org/10.56425/cma.v3i3.85

[12] K. Chang, X. Bai, J. Liu, , J. Wang, & X. Yan, Synchronous interlayer and surface engineering of NiFe layered double hydroxides by functional ligands for boosting oxygen evolution reaction, *Electrochimica Acta* **508** (2024) 145231. https://doi.org/10.1016/j.electacta.2024.145231

[13] H. He, J. Gu, X.Liu, D. Yang, Y. Zhu, R. Yao, Q. Fan, & R. Huang, Improvement of Trisodium Citrate-Modified NiFe-Layered Double Hydroxide Nanosheets with Carbon Black for Oxygen Evolution Reaction, *Catalysts* **10** (2020) 431. https://doi.org/10.3390/catal10040431

[14] J. Qu, Hu, Xiao & Deconinck, Marielle & Liu, Lixiang & Cheng, Yapeng & Zhao, Ruyan & Wang, Mingchao & Zhang, Haining & Vaynzof, Yana & Schuster, Jörg & Cabot, Andreu & Leistner, Karin & Li, Fei, Trisodium Citrate-Assisted Synthesis of Edge-Abundant Nickel-Iron Layered Double Hydroxides for Efficient Oxygen Evolution Reaction, *ChemCatChem* **17** (2024).

https://doi.org/10.1002/cctc.202401667.

[15] R. Abdel-Karim, Y. reda, M. Muhammed, S. El-Raghy, M. Shoeib, H. Ahmed, Electrodeposition and Characterization of Nanocrystalline Ni-Fe Alloys, *Journal of Nanomaterials* **2011** (2011). https://doi.org/10.1155/2011/519274

[16] A. Ayuningsih, Potentiostatic Electrodeposition of FeCo Thin Films: Influence of Deposition Temperature and Saccharin Concentration, Chemistry and Materials **4** (2025) 50-57.

[17] Y. Wu, B. Ji, W. Wang, Reducing the Internal Stress of Fe-Ni Magnetic Film Using the Electrochemical Method, Processes **9** (2021) 1883. https://doi.org/10.3390/pr9111883

[18] P. Tandon, R. Sahu, A. C. Mishra, K. Singh, Kavita Srikanti, R. Gopalan, Magnetoimpedance effect in electrodeposited NiFe/Cu wire using trisodium citrate additive in plating bath, *Journal of Magnetism and Magnetic Materials* **570** (2023). https://doi.org/10.1016/j.jmmm.2023.170490

[19] V.V. Kondalkara, X.Lia, S. Yanga, K. Leea, Current Sensor Based on Nanocrystalline NiFe/Cu/NiFe Thin Film, *Procedia Enginering* **168** (2016) 675-679. https://doi.org/10.1016/j.proeng.2016.11.245

[20] G.A. Gebreslase, D. Sebastián, M.V. Martínez-Huerta, M.J. Lázaro, Nitrogen-doped carbon decorated-$Ni_3Fe@Fe_3O_4$ electrocatalyst with enhanced oxygen evolution reaction performance, *Journal of Electroanalytical Chemistry* **925** (2022) 116887. https://doi.org/10.1016/j.jelechem.2022.116887

[21] N.Iqbal, S. Khan, & F. Ahmad, PZT and SrCeO as catalysts, their Synthesis and Applications in Alcohol Fuel Cell, *Journal of Medicinal and Nanomaterials Chemistry* **5** (2023) 186-198. doi: 10.48309/JMNC.2023.3.2

[22] J.I. Choi, I. Park, S. Park, M.J. Yi, W. Jang, J.H. Seo, Kinetic analysis of NiCo electrodeposition with saccharin using electrochemical impedance spectroscopy, *Electrochemistry Communications* **175** (2025) 107912. https://doi.org/10.1016/J.ELECOM.2025.107912

[23] O.v.d. Heijden, S. Park, R.E. Vos, J.J.J. Eggebeen, M.T.M. Koper, Tafel slope plot as a tool to analyze electrocatalytic reactions, *ACS Energy Letters* **9** (2024) 1871–1879. https://doi.org/10.1021/acsenergylett.4c00266

[24] Y. Uchida, E. Kätelhön, R.G Compton, Cyclic voltammetry with non-triangular waveforms: Electrochemically irreversible and quasi-reversible systems, *Journal of Electroanalytical Chemistry* **810** (2018) 135–144. https://doi.org/10.1016/j.jelechem.2017.12.053

[25] Y. Gao, Z. Zhao, H. Jia, X. Yang, X. Lei, X. Kong, F. Zhang, Partially reduced Ni2+, Fe3+-layered double hydroxide for ethanol electrocatalysis, *J. Mater. Sci.* **54** (2019) 14515–14523. https://doi.org/10.1007/s10853-019-03964-0

[26] J. Li, L. Li, X. Ma, J. Wang, J. Zhao, Y. Zhang, R. He, Y. Yang, A. Cabot, Y. Zhu, Unraveling the role of iron on Ni-Fe alloy nanoparticles during the elctrocatalytic ethanol-to-acetate process, *Nano Research* **17** (2024) 2328−2336. https://doi.org/10.1007/s12274-023-6049-4

[27] F. Lou, D. Chen, Aligned carbon nanostructures based 3D electrodes for energy storage, *Journal of Energy Chemistry* **24** (2015) 559–586. https://doi.org/10.1016/j.jechem.2015.08.013

[28] K.Y. Hwa, T.S.K. Sharma, Nano assembly of NiFe spheres anchored on *f*-MWCNT for electrocatalytic reduction and sensing of nitrofurrantoin in biological samples, *Scientific Reports*

[29] Q. Zhou,, C. Xu,, J Hou, W. Ma, T. Jian, S. Yan, H. Liu, Duplex Interpenetrating-Phase FeNiZn and FeNi3 Heterostructure with Low-Gibbs Free Energy Interface Coupling for Highly Efficient Overall Water Splitting, *Nano-Micro Lett.* **15** (2023). https://doi.org/10.1007/s40820-023-01066-w

[30] J. D.Lović, S. Eraković Pantović, L. Z. Rakočević, N. L. Ignjatović, S. B. Dimitrijević & N. D. Nikolić, A novel two-step electrochemical deposition method for Sn-Pd electrocatalyst synthesis for a potential application in direct ethanol fuel cells. *Processes* **11** (2023) 120 https://doi.org/10.3390/pr11010120.

[31] A. Kotelnikova, T. Zubar, T. Vershinina, M. Panasyuk, O.Kanafyev, V. Fedkin, & A. Trukhanov, The influence of saccharin adsorption on NiFe alloy film growth mechanisms during electrodeposition. *RSC advances* **12** (2022) 35722-35729. https://doi.org/10.1039/D2RA07118E

[32] M. Xi, Z. Liu, J. Ding, W. Cheng, D. Jia, & H. Lin, Saccharin anion acts as a “traffic assistant” of Zn2+ to achieve a long-life and dendritic-free zinc plate anode, *ACS Applied Materials & Interfaces* **13** (2021) 29631-29640. https://doi.org/10.1021/acsami.1c06307